

Work Extraction and Landauer's Principle in a Quantum Spin Hall Device

A. Mert Bozkurt,¹ Barış Pekerten,¹ and İnanç Adagideli^{1,*}

¹*Faculty of Engineering and Natural Sciences, Sabanci University, Orhanli-Tuzla, Istanbul, Turkey*
(Dated: June 12, 2018)

Landauer's principle states that erasure of each bit of information in a system requires at least a unit of energy $k_B T \ln 2$ to be dissipated. In return, the blank bit may possibly be utilized to extract usable work of the amount $k_B T \ln 2$, in keeping with the second law of thermodynamics. While in principle any collection of spins can be utilized as information storage, work extraction by utilizing this resource in principle requires specialized engines that are capable of using this resource. In this work, we focus on heat and charge transport in a quantum spin Hall device in the presence of a spin bath. We show how a properly initialized nuclear spin subsystem can be used as a memory resource for a Maxwell's Demon to harvest available heat energy from the reservoirs to induce charge current that can power an external electrical load. We also show how to initialize the nuclear spin subsystem using applied bias currents which necessarily dissipate energy, hence demonstrating Landauer's principle. This provides an alternative method of "energy storage" in an all-electrical device. We finally propose a realistic setup to experimentally observe a Landauer erasure/work extraction cycle.

PACS numbers: 74.78.Na, 85.75.-d, 72.10.-d

I. INTRODUCTION

According to Landauer's principle, erasure of one bit of information requires an amount of heat greater than $k_B T \ln 2$ to be dissipated^{1,2}. The principle ensures that the second law of thermodynamics is obeyed as a blank bit is utilized to extract work by an amount $k_B T \ln 2$ from the environment. The "engine" that is capable of this extraction is sometimes called a "Maxwell's Demon" (MD), referring to the thought experiment proposed by Maxwell in 1871³. While interest in MD and Landauer's principle from the point of view of fundamental physics never faded⁴⁻⁹, promise of highly efficient engines that operate in the nano-domain¹⁰⁻¹² as well as alternative methods of energy storage gave a recent impetus to research on the physics of MD both experimentally (using colloidal particles¹³⁻¹⁵, photonic systems^{16,17}, NMR systems^{18,19}, single electron transistors²⁰⁻²³, cavity QED with superconducting qubits²⁴) and theoretically²⁵⁻⁴⁰. Despite the multitudinous platforms in which MD action is theorized or demonstrated, scalability remains an issue.

In this manuscript, we propose and investigate a new MD implementation that harvests thermal energy from the electronic environment and converts it to electrical work using a quantum spin Hall insulator (QSHI). As a memory resource we use the available nuclear spins present in the device and/or magnetic impurities introduced via doping. QSHIs feature an insulating bulk and a pair of counter-propagating gapless spin-momentum locked helical edge states that are topologically protected from backscattering under time-reversal symmetry (TRS)⁴¹ (see Fig. 1). First predicted to exist in graphene nanoribbons^{42,43}, they were later experimentally found in HgTe/CdTe quantum wells (QWs)^{44,45} as well as in InAs/GaSb QW structures^{46,47}. The TRS prohibiting the backscattering of the edge states is broken by the presence of nuclear or impurity spins. This backscatter-

ing shows up as extra dissipation, lowering the expected quantized conductance of the QSHI edge⁴⁸⁻⁵². Here we show another salient feature of such scattering: an initial state of polarized nuclear spins (blank memory) drives an electric current. Thus nuclear/impurity spins act as a memory resource of a MD that converts heat from the environment into electrical work.

We show below that for the heat harvesting operation of our engine, no energy exchange between nuclear and electronic systems is necessary; in fact, the nuclear spins are degenerate in our system, forming a non-energetic (pure) memory. Hence this is an alternative way for energy storage (Fig. 2) that is protected from undesired explosive discharges. The total energy needed to reset the "memory" (or, in other words, recharge the device) by fully polarizing nuclear spins exceeds the extracted energy, in agreement with the second law of thermodynamics and Landauer's principle. We also provide a method to generate such a nuclear spin polarization, completing the discharge-recharge cycle of the quantum information engine (QIE) (Fig. 2). We note that each nucleus with nonzero nuclear spin coupling to the electron spin in the QSHI edge contributes to the MD memory, hence the MD memory size here could be several orders of magnitude larger compared to those that were reported in the literature, thus solving the scaling problem for heat harvesting engines. Furthermore, our estimates show that equivalent energy/power density of our proposed engine compares favourably with conventional energy storage such as supercapacitors.

II. NUCLEAR SPINS IN QUANTUM SPIN HALL INSULATORS

We now describe the basic model of our MD implementation. The effective dynamics of electrons and holes

in QSHI materials is well described by the Bernevig-Hughes-Zhang (BHZ) Hamiltonian⁴⁴:

$$\mathcal{H}_{\text{BHZ}} = \epsilon_k \sigma_0 \tau_z + E_k \sigma_0 \tau_0 + A (k_x \sigma_z \tau_x - k_y \sigma_0 \tau_y), \quad (1)$$

where $\epsilon_k = M - Bk^2$, $E_k = C - Dk^2$ and M , A , B , C , D are the material parameters. The BHZ Hamiltonian acts on the envelope wave functions $(\psi_{+,E}, \psi_{-,E}, \psi_{+,H}, \psi_{-,H})^T$, where $\sigma = \pm$ denote the spin, $\tau = E, H$ denote the electron-hole degrees of freedom and σ_α and τ_α ($i \in \{x, y, z\}$) are the Pauli matrices that act in spin and electron-hole spaces respectively. (We also define the corresponding unit matrices σ_0 and τ_0 .) In order to describe the coupling to nuclear spins we also need the full wavefunction which includes the lattice-periodic factors⁵³:

$$\Psi(\vec{r}) = \sum_{\sigma, \tau} \psi_{\sigma, \tau}(\vec{r}) u_{\sigma, \tau}(\vec{r}). \quad (2)$$

In this description, the various two-dimensional QSHI QW structures differ only in their material and effective parameters⁵⁴, while the main edge state physics remains the same (Fig. 1a). The low energy excitations in the topological phase are localized to the edges of the system. These excitations are called helical edge states and their wavefunctions have the general form :

$$\psi_{\sigma, \tau}^{\pm}(\vec{r}) = \xi(\vec{r}_\perp) \phi^{\pm}(x), \quad (3)$$

where the superscript \pm denotes the edge states of different chiralities. In the absence of spin-orbit coupling, the chiralities are specified by their spin so that $\psi_{\sigma, \tau}^{\pm} \propto \delta_{\pm, \sigma}$. (Note that in the presence of spin-orbit coupling, the spin axes becomes position dependent⁵⁵.) We next project the electronic Hilbert space to the space spanned by the edge states given in Eq. 3 above, obtaining the projected electron Hamiltonian which reads $h_{\text{bot(top)}}^{\text{eff}} = \mp i \hbar v_F \partial_x \sigma_z$. Here, v_F is the Fermi velocity of the effective edge state and \pm signs refer to the top (+) and the bottom (-) edge (see Fig. 1b).

The second important element in our QIE is the nuclear spin subsystem that forms the “memory” of the MD that operates on electron-hole dynamics via their spins. We model the interaction between the spins of the nuclei and the spins of the electrons by the Fermi contact hyperfine interaction⁵⁶, which is given by

$$H_{\text{hf}} = v_0 \sum_{i=1}^N A_i \delta(\vec{r} - \vec{R}_i) \vec{I}_i \cdot \vec{\sigma}, \quad (4)$$

where $\vec{\sigma}$ are the electron spin operators, v_0 is the volume of the unit cell of the corresponding QSHI component material, \vec{I}_i is the nuclear spin operator at position \vec{R}_i and A_i is the hyperfine coupling energy. The total low energy effective Hamiltonian including the hyperfine interaction projected to the edge states is then given by

$$H_{\text{bot(top)}} = (\mp i \hbar v_F \partial_x + \lambda M_z(x)) \sigma_z$$

$$H_{\text{s-flip}} = \sum_{i=1}^N \frac{\lambda_i}{2} \delta(x - x_i) (I_{i+} \sigma_- + I_{i-} \sigma_+), \quad (5)$$

where x denotes the position along the edge in consideration. In this effective Hamiltonian given in Eq. (5), the electrons interact with all the nuclear spins within the cross section of the helical edge states, which we denote as S . We further assume for simplicity that the effective hyperfine coupling $\lambda_i = \lambda$ is constant for all sites, which does not qualitatively alter the physics, and estimate its value as $\lambda = A_0 v_0 / S$, where A_0 is the average value of A_i . In anticipation of dynamically polarized nuclear states that we will consider below, we have also introduced $M_z(x)$ as the z -component of the Overhauser field⁵⁶. We note that $M_z(x)$ can be gauged away via $H_{\text{bot(top)}} \rightarrow U H_{\text{bot(top)}} U^\dagger$ with $U = \exp(\frac{\pm i \lambda}{\hbar v_F} \int^x M_z(x') dx')$.

We note that because the spin of the electron and its momentum is completely locked, as $H_{\text{s-flip}}$ flips the spin of the edge electron and one nuclear spin, it also causes backscattering (see Fig. 1d). We assume that the temperature of the system is higher than T^* , below which RKKY and other nuclear correlation effects become important. T^* is estimated to be around 100 mK or less⁵². The Fermi contact interaction process runs in competition with other processes that affect the nuclear spins, mainly the quadrupole interaction causing spin-flip between nuclear spins. However, the rate of this interaction is orders of magnitude smaller than the spin-flip rate from the coupling between nuclear and electronic spins⁵⁷.

III. CHARGING/DISCHARGING CYCLE OF QIE

In this section, we describe the charging/discharging (or alternatively erasure/work extraction) operation. In the charging phase, we apply a charge current, which without loss of generality we assume to be flowing to the left, leading to more right movers than left movers, and hence to more right to left backscattering. In the bottom edge, right movers are spin up electrons. Thus the backscattering creates up-nuclear spins from spin-flip scattering. In the top edge right movers are spin down electrons hence the backscattering creates down-nuclear spins (see Fig. 2b). This process polarizes the nuclear spins until a certain net bias-dependent value is reached^{48,50}. This is the process of dynamical nuclear polarization for the quantum spin Hall edges, well-known in other contexts such as spin injection from ferromagnets^{58,59}. We stress that under a current bias, opposite edges are driven towards opposite polarization values.

More importantly, the reverse process is also possible: fully polarized nuclear spins near a QSHI edge drive a charge current (see Fig. 2c). This is the discharging phase. Consider a nonzero initial nuclear spin polarization with opposite signs in opposite edges (caused by, say, the driving current described above) and for simplicity assume zero applied voltage bias. Now there are more up[down]-nuclear spins than down[up]-nuclear spins in the bottom[top] edge, hence there are more down[up]-spins flipped to up[down]-spins in the bottom[top] edge,

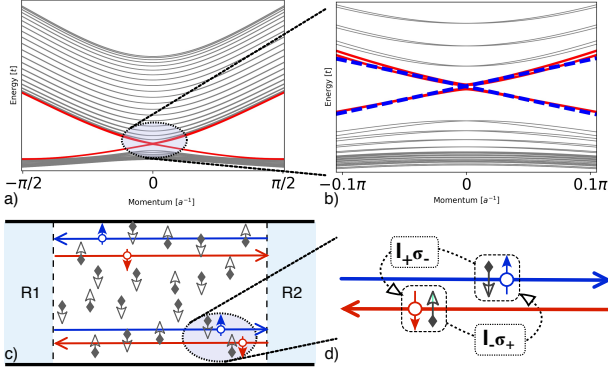


FIG. 1. (Color online) QSHI with nuclear spins and electron-nuclear spin flip interaction. (a) The band structure of a typical QSHI system (using the BHZ model with tight-binding approximation). Red lines represent the edge states. (b) The band structure of the simplified Hamiltonian h_{eff} projected to a single edge (dashed blue lines). (c) Schematic description of the QSHI system with the edge currents interacting with the nuclear spins in the system, with the diamonds representing nuclear spins. (d) The spin flip interaction with the nuclear spins that form the MD.

leading to an imbalance of left movers relative to right movers. Any time a backscattering occurs, the event leaves its footprint via a spin-flip in the nuclear memory. A reverse bias can now be applied so that the current is opposite of the voltage bias in order to extract work. We show below that the energy is supplied by the thermal energy of the reservoirs. All this is reminiscent of a MD operation wherein the MD predominantly backscatters the right movers relative to the left movers, thus setting up a current between reservoirs that are otherwise in equilibrium, while recording the outcome in the nuclear spin memory (see Fig. 2). Under applied reverse bias, the MD/QIE harvests heat to convert it to electrical work.

A. Polarization dynamics and induced current

We now quantify our model. The dynamics of the edge electrons are modified in the presence of nuclear spins via the spin-flip scattering which can be calculated using Fermi's golden rule in terms of the electron density matrix $\rho(r, r')$. For ease of notation, we now focus on the bottom edge, where all right moving electrons have spin up and left movers have spin down. The top edge results can be obtained by substituting: spin down \rightarrow spin up and vice versa. Then, the scattering rate from right to left (with accompanying nuclear spin flips) between x and $x + \Delta x$ is given by^{48,50}:

$$\Gamma_{-+}(\epsilon, x) = \frac{\gamma_0}{\hbar} N_{\downarrow}(x) f_{+}(\epsilon, x) (1 - f_{-}(\epsilon, x)), \quad (6)$$

where $N_{\downarrow}(x)$ is the number of nuclear down spins between x and $x + \Delta x$, $\gamma_0 \equiv \lambda^2 / 8\pi \hbar^2 v_F^2$ is a dimensionless

effective electron spin-nuclear spin interaction strength. Here, $f_{\pm}(\epsilon, x)$ are the distributions of right[left] movers with energy ϵ at position x along the edge and are given in terms of the Wigner transform of the density matrix $\rho_{\pm}(r, r')$ of the right and left moving electrons as:

$$f_{\pm}(\epsilon, x) = \int dr \rho_{\pm}(x + r/2, x - r/2) e^{\pm i\epsilon r / \hbar v_F}. \quad (7)$$

1. Nuclear polarization dynamics

The effect of spin-flip scattering on the nuclear spins is given by the rate equation:

$$\frac{dN_{\uparrow}(x)}{dt} = \int d\epsilon (\Gamma_{-+}(\epsilon, x) - \Gamma_{+-}(\epsilon, x)). \quad (8)$$

We find it useful to define the mean polarization $m(x) \equiv \frac{N_{\uparrow}(x) - N_{\downarrow}(x)}{2(N_{\uparrow}(x) + N_{\downarrow}(x))}$, whose time rate of change is

$$\frac{dm(x)}{dt} = \gamma_0 \Gamma_B(x) - m(x) \gamma_0 \Gamma_T(x) \quad (9)$$

with $\hbar \Gamma_B(x) = \int d\epsilon (f_{+}(\epsilon, x) - f_{-}(\epsilon, x)) / 2$ and $\hbar \Gamma_T(x) = \int d\epsilon (f_{+}(\epsilon, x) + f_{-}(\epsilon, x) - 2f_{+}(\epsilon, x)f_{-}(\epsilon, x))$. For the rest of the paper we focus on a short edge, where the weak dependence of f_{\pm} and m on x can be ignored. Hence, we approximate $m(x)$ by its leading, x -independent, order. We also approximate the distributions $f_{+}(\epsilon, x)$ of the right movers and $f_{-}(\epsilon, x)$ of the left movers by the Fermi distributions $f_L^0(\epsilon)$ and $f_R^0(\epsilon)$ of the reservoirs from which they originate (see Appendix A). We therefore get

$$\begin{aligned} \hbar \Gamma_B &= (\mu_L - \mu_R) / 2, \\ \hbar \Gamma_T &= (\mu_L - \mu_R) \coth\left(\frac{\mu_L - \mu_R}{2k_B T}\right), \end{aligned} \quad (10)$$

where $\mu_L[\mu_R]$ is the chemical potential of the left[right] reservoir. We now use these expressions in Eq. (9) to obtain the time dependence of the polarization:

$$m(t) = (m_0 - \bar{m}) e^{-t/\tau_m} + \bar{m}, \quad (11)$$

where m_0 is the initial mean polarization and $\bar{m} \equiv \Gamma_B / \Gamma_T = (1/2) \tanh\left(\frac{\mu_L - \mu_R}{2k_B T}\right)$ is defined to be the target mean polarization and $\tau_m = 1/\gamma_0 \Gamma_T$ is the characteristic time scale for nuclear polarization dynamics.

2. Electron dynamics and induced current

We now calculate the total current. The distribution functions obey the Boltzmann-like equation for the bottom edge:

$$\partial_t f_{\pm} = \pm (\Gamma_{+-}(\epsilon, x) - \Gamma_{-+}(\epsilon, x)) \nu(0)^{-1} \mp v_F \partial_x f_{\pm}, \quad (12)$$

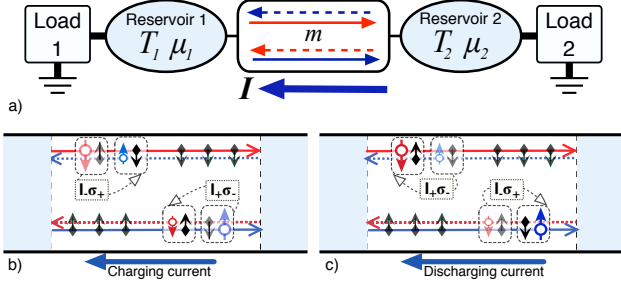


FIG. 2. (Color online) a) QSHI based quantum information engine, providing power to loads 1 and 2. Schematic description of b) the charging and c) the discharging phase of the QIE. In the charging phase, an applied bias current increases the number of right-movers (solid lines) at the edges relative to left-movers (dashed lines). This excess in turn creates a net nuclear spin polarization with opposite values in each edge. In the discharging phase, even without external bias, the net polarization of the nuclear spins increases the number of right-movers, driving a net discharging current to the left.

where $\nu(0) = L/2\pi\hbar v_F$ is the density of states of the edge electrons. We assume that the nuclear polarization m is changing slowly and seek a steady state solution. Then the distributions obey:

$$\begin{aligned} \partial_x f_{\pm} &= (\Gamma_{+-}(\epsilon, x) - \Gamma_{-+}(\epsilon, x)) (v_F \nu(0))^{-1} \\ &\equiv \Gamma[f_+, f_-] \end{aligned} \quad (13)$$

For short edges ($\Gamma[f_+, f_-]L \ll 1$), we expand in gradients of the distribution functions. At the leading order, we obtain a linear position dependence:

$$f_{\pm} = f_{L(R)}^0(\epsilon) + \Gamma[f_L^0(\epsilon), f_R^0(\epsilon)](x \pm L/2). \quad (14)$$

We then obtain the total current (see Appendix A):

$$I_{tot} = \frac{e}{h} \int d\epsilon (f_+ - f_-) = \frac{e^2}{h} V - eN\gamma_0(\Gamma_B - m\Gamma_T). \quad (15)$$

We identify and focus on two sources of current in the system in the short edge regime: (i) the usual current $\frac{e^2}{h}V$ due to voltage bias without the nuclear spin-flip interaction, and (ii) the MD-induced current $-eN\frac{dm}{dt} = -eN\gamma_0(\Gamma_B - m\Gamma_T)$ due to the presence of nuclear polarization m . In the latter case, a net backscattering current, caused by right-moving up-spin electrons scattering to left-moving down-spin electron states, is driven by a net negative nuclear spin and vice versa. We note that the net polarization of the nuclear spins acts as a Maxwell's Demon: The total current is nonzero for vanishing bias voltage, demonstrating the “Demon action” that induces a current between two reservoirs at equal temperature and chemical potential, while using the nuclear spins as a memory resource.

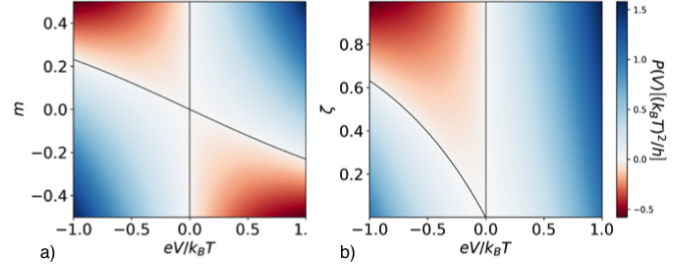


FIG. 3. (Color online) Power, calculated using Eq. (16), as a function of the applied voltage and a) as a function of mean polarization m with $\zeta = 1.0$ and b) as a function of ζ with full polarization $m = 0.5$. The lines divide the charging ($P > 0$) and discharging ($P < 0$) phases. Power can have negative values for $V < 0$ ($V > 0$) for a given mean polarization $m > 0$ ($m < 0$) (here, $e > 0$), as an indication of the work extraction phase.

B. Generated power and extracted work

In order to use the quantum information engine, we attach it to an electrical circuit as in Fig. 2. In this setup, the QIE provides power to loads 1 and 2, which can be modeled by a (reverse) bias voltage V . The power generated (Fig. 3) is given by:

$$P = \frac{eV}{h} \left(eV(1 - \frac{\zeta}{2}) + \zeta \hbar \Gamma_T m \right), \quad (16)$$

with $\zeta = 2\pi N\gamma_0$. For $eV < \frac{2\zeta\hbar\Gamma_T m}{(\zeta-2)}$, we obtain $P < 0$, indicating that the circuit is powered by the QIE. (For $eV > \frac{2\zeta\hbar\Gamma_T m}{(\zeta-2)}$, the circuit is providing power to charge the nuclear spin resource). We find the maximal work done by the nuclear spin resource in the weak coupling/short edge limit by maximizing the power and integrating up to the time when the power changes sign⁶⁰:

$$W_{tot} = \alpha k_B T N^2 \gamma_0, \quad (17)$$

where α is a parameter of $\mathcal{O}(1)$ (a detailed calculation produces $\alpha = \pi/4$ for a work extraction under constant voltage bias (see Appendix B). In this limit, the amount of extracted work follows a quadratic scaling law that implies denser storage than the conventional/expected linear scaling. Here, T is the operating temperature, limited by the bulk band gap of the QSHI. We find that the inequality

$$P + k_B T \dot{S}_{nuc} \geq 0, \quad (18)$$

where S_{nuc} is the information entropy of the nuclear spin subsystem, is satisfied in agreement with the second law of thermodynamics (see Appendix C).

C. Physical implementation

We now discuss experimental feasibility of our MD implementation. Systems featuring spin-momentum locked

topological edge states have been available to experiments for about a decade^{61,62}. Among these materials, systems with high nuclear spin density generally provide high energy density. In addition, systems with higher bulk bandgaps could be operated at higher temperatures, again leading to higher energy densities (see Eq. (17)). Systems that feature high hyperfine interaction strength or low Fermi velocity provide high power density and fast operation, thus can be utilized as spin-supercapacitors. Assuming $N \sim 10^7$ and $\gamma_0 \sim 10^{-8}$, we estimate the equivalent energy density and power density that can be stored in the device in the short edge limit to be $\sim 10\text{kJ/kg}$ and $\sim 10\text{MW/kg}$ (not including overhead). On the other hand, systems with low interaction strength (see Eq. (6)) due to high Fermi velocity and/or suppressed hyperfine interaction can be utilized as spin batteries that keep their polarization for long times. For example, thin film flakes of 3D topological QSHI $\text{Bi}_2\text{Te}_2\text{Se}$ (BTS221) feature a relatively large Fermi velocity ($v_F \sim 10^6\text{m/s}$)⁶³, which is two orders of magnitude larger than that of, say, InAs/GaSb QWs ($v_F \sim 10^4\text{m/s}$)⁴⁷. Thus, BTS221 features a much smaller electron-nuclear spin-flip interaction strength (therefore requiring large currents to write the spin memory) and orders of magnitude longer memory retention times. In fact, recent experimental work that uses thin film flakes of BTS221 observed days long polarization retention times⁶⁴.

We next consider InAs/GaSb QW structures as an example. These QWs have a smaller Fermi velocity v_F ^{41,47} and higher nuclear spin density compared to, for example, HgCdTe QWs⁵³. This hints to a larger $N\gamma_0$ in InAs/GaSb QWs and therefore to a faster operation and higher energy density. We note that in these QWs, the electrons have spin $\pm 1/2$ but the holes have spin $\pm 3/2$ whose coupling to the spin-flip interaction requires a higher order process⁵³. The nuclear spin density in these QWs, as well as the effective electron spin-nuclear spin coupling strength, could possibly be further adjusted by magnetic impurity doping, providing a design freedom that might prove useful for different functionalities of the QIE.

IV. CONCLUSION

In summary, we have described a Maxwell's Demon system that utilizes the spin-flip interaction between helical edge states and nuclear spins in quantum spin Hall topological insulators. Available nuclear or magnetic impurity spins can be utilized as a Maxwell's Demon memory to harvest work from thermal energy of the reservoirs. We also showed how to erase the memory and thus "charge" the system by applying a voltage bias. Erasing the memory (or polarizing the spin subsystem) requires dissipation of heat by an amount at least $k_B T \ln 2$ per bit, in agreement with the Landauer's principle and the second law. Estimates of equivalent work that can be

extracted show that power/energy densities that exceed existing supercapacitors are achievable.

ACKNOWLEDGMENTS

We thank İ. İ. Kaya, J. Vaccaro and Ö. Müstecaplıoğlu for discussions. We especially thank N. Allen for inspiration as well as many fruitful discussions throughout this work. IA is a member of the Science Academy-Bilim Akademisi-Turkey; BP and AMB thank The Science Academy-Bilim Akademisi-Turkey for the use of their facilities. This research was supported by a Lockheed Martin Corporation Research Grant. IA and BP also acknowledge support by COST Action MP1209.

Appendix A: Mean Polarization Dynamics and Electric Current

In this appendix, we focus on the time dependence of the nuclear mean polarization and later obtain electric current in the short edge limit. We first define the mean polarization at position x per edge,

$$m(x) \equiv \frac{N_\uparrow(x) - N_\downarrow(x)}{2N(x)},$$

where $N(x) = N_\uparrow(x) + N_\downarrow(x)$ is the number of nuclei at position x and $x + \Delta x$ per edge participating in the spin-flip interactions. With this definition fully polarized nuclear spins have $m = \pm 1/2$.

The dynamics of the mean polarization, given in Eq. (9) and repeated below, is obtained from Eq. (6) and (8):

$$\frac{dm(x)}{dt} = \gamma_0 \Gamma_B(x) - m(x) \gamma_0 \Gamma_T(x). \quad (9)$$

As mentioned in the main text, $\Gamma_B(x)$ and $\Gamma_T(x)$ is given as:

$$\begin{aligned} \Gamma_B(x) &= \int \frac{d\epsilon}{\hbar} \frac{f_+ - f_-}{2} \\ \Gamma_T(x) &= \int \frac{d\epsilon}{\hbar} (f_+ + f_- - 2f_+ f_-), \end{aligned} \quad (A1)$$

where we suppressed the energy and position dependence of the distribution functions $f_\pm(\epsilon, x)$. Note that current conservation requires $\Gamma_B(x)$ to be x -independent.

For short edges we have $\Gamma[f_+, f_-] L \ll 1$, and $N_{\uparrow(\downarrow)}(x)$ and $m(x)$ have only a weak dependence on x . Performing a gradient expansion, we first approximate $N_{\uparrow(\downarrow)}(x)$ and $m(x)$ with their leading, x -independent, terms. We next approximate the distributions f_\pm with the Fermi distributions of the reservoirs $f_{L(R)}^0$ from which they originate. We now evaluate the integrals in Eq. (A1) and obtain

$$\begin{aligned} \Gamma_B &= (\mu_L - \mu_R)/2\hbar, \\ \Gamma_T &= \frac{(\mu_L - \mu_R)}{\hbar} \coth\left(\frac{\mu_L - \mu_R}{2kT}\right), \end{aligned} \quad (A2)$$

in agreement with Eq. (10). We note that in this approximation, Γ_B is proportional to the applied bias $\mu_L - \mu_R$, hence it vanishes for zero applied voltage. We also note that $\Gamma_T \geq 0$.

We now focus on the total current. In the short edge limit, the distribution functions of the right and left movers within the edge in question are given by Eq. (14). We then obtain the total current as

$$\begin{aligned} I_{tot} &= \frac{e}{h} \int d\epsilon (f_+ - f_-) \\ &= \frac{e}{h} \int d\epsilon \left[(f_L^0 - f_R^0) - h(\Gamma_{-+}(\epsilon) - \Gamma_{+-}(\epsilon)) \right] \\ &= \frac{e^2}{h} V - eN \frac{dm}{dt}, \end{aligned}$$

consistent with Eq. (15). Here, f_+ [f_-] are the (in general x -dependent) distribution functions of the right [left] movers in the given edge, and f_L^0 [f_R^0] are the (Fermi) distributions of the lead from which the right [left] movers originate. In the last line, we used Eq. (8) in the short edge limit. We identify the first term on the right hand side as the current due to the usual voltage bias (I_{bias}) and the second term as the induced current due to Maxwell's demon effect (I_{MD}).

In order to see the mean polarization dependence of the total current in the short edge limit, we substitute the explicit forms of Γ_B and Γ_T given in Eq. (10) into Eq. (15) to obtain:

$$I_{tot}(t) = \frac{e^2}{h} V \left[\left(1 - \frac{\zeta}{2} \right) + m(t) \zeta \coth \left(\frac{eV}{2kT} \right) \right], \quad (\text{A3})$$

where we defined a dimensionless quantity $\zeta = 2\pi N\gamma_0$, which is a rough measure of the interaction strength over the whole wire per edge. We see that in the limit of vanishing voltage bias, total current is not zero if $m(t)$ is nonzero. This behaviour persists even if the temperature or the chemical potential of both of the reservoirs are equal, demonstrating the pure entropy-driven current.

Appendix B: Work Extraction and Heat Dissipation

We calculate the power absorbed/generated by QIE under fixed applied voltage bias as follows:

$$\begin{aligned} P(t) &= I_{tot}(t) V \\ &= \frac{eV}{h} \left[eV \left(1 - \frac{\zeta}{2} \right) + \zeta m(t) h\Gamma_T \right] \\ &= \frac{eV}{h} \left[eV + \zeta(m_0 - \bar{m}) e^{-t/\tau_m} h\Gamma_T \right], \quad (\text{B1}) \end{aligned}$$

where in the last line we used Eq. (11) and $\bar{m}h\Gamma_T = \frac{eV}{2}$.

Charging cycle. We would like to find the amount of heat dissipated while we charge the device. Starting from

totally unpolarized nuclear spins ($m_0 = 0$) and using Eq. (11) and Eq. (B1), we get:

$$\begin{aligned} P(t) &= \frac{eV_C}{h} \left[eV_C - \zeta \bar{m} e^{-t/\tau_m} h\Gamma_T \right], \\ &= \frac{eV_C}{h} \left[eV_C - eV_C \frac{\zeta}{2} e^{-t/\tau_m} \right]. \quad (\text{B2}) \end{aligned}$$

As shown in Eq. (11), the amount of time to reach the target mean polarization is infinitely long. Instead, we charge the device up to a fraction of full polarization $m = \frac{\kappa}{2}$ where κ is a value we later choose depending on the application and whether we intend to maximize power or efficiency. Using $\frac{\kappa}{2} = \bar{m}(1 - e^{-\bar{t}/\tau_m})$, we obtain the following for the amount of time \bar{t} to reach the specified target mean polarization:

$$\bar{t} = -\tau_m \ln \left(1 - \frac{\kappa}{2\bar{m}} \right). \quad (\text{B3})$$

We then get the dissipated heat by integrating the power up to \bar{t} :

$$\begin{aligned} W_C(V_C) &= \int_0^{\bar{t}} \frac{eV_C}{h} \left[eV_C - \frac{\zeta}{2} e^{-t/\tau_m} eV \right] \\ &= \frac{e^2 V_C^2}{h} \tau_m \left[-\ln \left(1 - \frac{\kappa}{2\bar{m}} \right) - \frac{\zeta}{2} \frac{\kappa}{2\bar{m}} \right] \\ &= \frac{eV_C}{2\pi\gamma_0} \tanh \left(\frac{eV_C}{2k_B T} \right) \\ &\quad \times \left[\ln \left(\frac{2\bar{m}}{2\bar{m} - \kappa} \right) - \frac{\zeta}{2} \frac{\kappa}{2\bar{m}} \right]. \quad (\text{B4}) \end{aligned}$$

Note that $0 \leq 1 - \kappa/2\bar{m} < 1$. This condition gives us a lower bound on the applied voltage:

$$V_C \geq \frac{k_B T}{e} \ln \left(\frac{1 + \kappa}{1 - \kappa} \right). \quad (\text{B5})$$

Discharging cycle. For the next step in the engine cycle, we apply a reverse (discharging) bias, $V_D < 0$, and we would like to find the time t^* at which $P(t)$ changes sign. Using Eq. (B1), we obtain:

$$t^* = \tau_m \ln \left[\zeta \left(\frac{1}{2} + m_0 \coth \left(\frac{|eV_D|}{2k_B T} \right) \right) \right] \quad (\text{B6})$$

We then integrate the power up to $t = t^*$ to obtain the work done at fixed voltage:

$$\begin{aligned} W_D(V_D) &= \int_0^{t^*} \frac{|eV_D|}{h} \left[|eV_D| - \zeta(m_0 - \bar{m}) e^{-t/\tau_m} h\Gamma_T \right] \\ &= \frac{e^2 V_D^2}{h} t^* \\ &\quad + \frac{|eV_D|}{h} \tau_m \zeta (m_0 - \bar{m}) h\Gamma_T (e^{-t^*/\tau_m} - 1). \quad (\text{B7}) \end{aligned}$$

Inserting t^* into the equation above and using the relation $\bar{m}\hbar\Gamma_T = -\frac{|eV_D|}{2}$, we get:

$$W_D(V_D) = \frac{e^2 V_D^2}{h} \tau_m \left[\ln \left(\frac{\zeta}{2} + m_0 \zeta \coth \left(\frac{|eV_D|}{2k_B T} \right) \right) + 1 - \left(\frac{\zeta}{2} + m_0 \zeta \coth \left(\frac{|eV_D|}{2k_B T} \right) \right) \right]. \quad (\text{B8})$$

We finally take the polarization reached at the end of the charging cycle, $m_0 = \frac{\kappa}{2}$, as the initial polarization for the discharging cycle to finally obtain

$$W_D(V_D) = \frac{|eV_D|}{2\pi\gamma_0} \tanh \left(\frac{|eV_D|}{2k_B T} \right) \times \left[\ln \left(\frac{\zeta}{2} + \frac{\kappa\zeta}{2} \coth \left(\frac{|eV_D|}{2k_B T} \right) \right) + 1 - \left(\frac{\zeta}{2} + \frac{\kappa\zeta}{2} \coth \left(\frac{|eV_D|}{2k_B T} \right) \right) \right]. \quad (\text{B9})$$

In order to extract work from the nuclear spin polarization, one has to make sure that $t^* > 0$, which gives us an upper bound on the applied voltage:

$$|V_D| \leq \frac{k_B T}{e} \ln \left(\frac{2 - \zeta(1 - \kappa)}{2 - \zeta(1 + \kappa)} \right). \quad (\text{B10})$$

Maximum Work Extraction: Eq. (B10) suggests that, in the short edge limit, work extraction is only possible when the applied reverse bias is smaller than the thermal energy. We therefore consider the $2k_B T \gg |eV_D|$ case and approximate Eq. (B9) as follows:

$$W_D(V_D) \approx \frac{|eV_D|^2}{4k_B T \pi \gamma_0} \left[\ln \left(\frac{\zeta}{2} \left(1 + \kappa \frac{2k_B T}{|eV_D|} \right) \right) + 1 - \frac{\zeta}{2} \left(1 + \kappa \frac{2k_B T}{|eV_D|} \right) \right]. \quad (\text{B11})$$

The maximum work that can be extracted from QIE can be obtained by maximizing Eq. (B9) with respect to applied reverse bias V_D . We neglect the logarithmic term in Eq. (B9) and we find the applied reverse bias that maximizes the amount of extracted work:

$$|eV_D^*| = \frac{k_B T \zeta \kappa}{(2 - \zeta)}. \quad (\text{B12})$$

Plugging V_D^* into Eq. (B11) and choosing maximum initial polarization $\kappa = 1$, we get the maximum work that

can be extracted under constant voltage bias in the short edge limit as:

$$W_{tot} \simeq \frac{\pi}{4} k_B T N^2 \gamma_0. \quad (\text{B13})$$

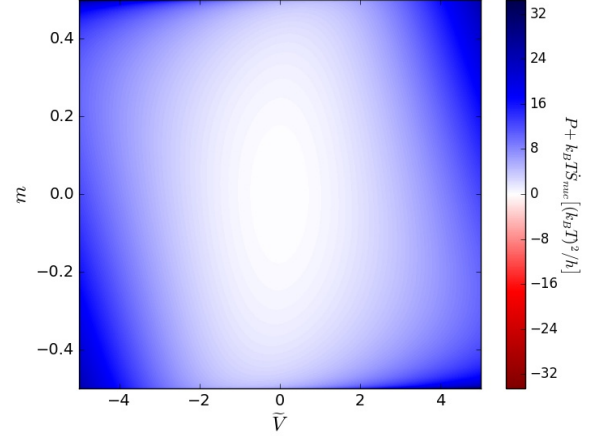


FIG. 4. (Color online) $P + k_B T \dot{S}_{nuc}$ as a function of \tilde{V} and m for $\zeta = 1$. Note that $P + k_B T \dot{S}_{nuc} \geq 0$, in agreement with the second law.

Appendix C: Information Entropy and the Second Law of Thermodynamics

The second law of thermodynamics in our context can be restated as

$$\beta P + \frac{d}{dt} S_{nuc} \geq 0, \quad (\text{C1})$$

where $\beta \equiv (k_B T)^{-1}$ and P is the power dissipated at (extracted from) the reservoirs, T is the ambient temperature and S_{nuc} is the information entropy of the nuclear spin subsystem. As we extract work using nuclear spins as a memory resource ($P < 0$), we see that the information entropy of the nuclear spin subsystem has to increase. In the reverse process in which we erase the memory ($P > 0$), the information entropy of the nuclear spin subsystem decreases, which corresponds to the Landauer's erasure principle.

For our system, i.e. QIE in the short edge limit, we use Eq. (B1) and obtain

$$\beta P + \dot{S}_{nuc} = \frac{1}{\beta \hbar} [\tilde{V}^2 + \zeta \tilde{V} (\tilde{V} + X) \times (m \coth \frac{\tilde{V}}{2} - \frac{1}{2})] \geq 0, \quad (\text{C2})$$

where $\tilde{V} \equiv \beta eV$ and $X = \ln \left(\frac{1+2m}{1-2m} \right)$, in agreement with the second law of thermodynamics (see Fig. 4).

* adagideli@sabanciuniv.edu

¹ R. Landauer, IBM J. Res. Devel. **3**, 183 (1961).

- ² C. H. Bennett, Int. J. Theor. Phys. **21**, 905 (1982).
- ³ H. S. Leff and A. F. Rex, *Maxwell's Demon 2* (IOP Publishing, Bristol, 2003); K. Maruyama, F. Nori and V. Vedral, Rev. Mod. Phys. **81**, 1 (2009).
- ⁴ S. Lloyd, Phys. Rev. A **56**, 3374 (1997).
- ⁵ M. O. Scully, Phys. Rev. Lett. **87**, 220601 (2001).
- ⁶ T. D. Kieu, Phys. Rev. Lett. **93**, 140403 (2004).
- ⁷ J. A. Vaccaro and S. M. Barnett, Proc. R. Soc. A, **467**, 1770, (2011).
- ⁸ S. M. Barnett and J. A. Vaccaro, Entropy, **15**, 4956, (2013).
- ⁹ T. Croucher, S. Bedkihal, J. A. Vaccaro, Phys. Rev. Lett. **118**, 060602 (2017).
- ¹⁰ S. Datta, *Lecture Notes in Nanoscale Science and Technology, Vol. 2, Nanoscale Phenomena: Basic Science to Device Applications*, Eds. Z.K. Tang and P. Sheng, Springer (2008).
- ¹¹ R. Bustos-Marín, G. Refael, and F. von Oppen, Phys. Rev. Lett. **111**, 060802 (2013).
- ¹² L. Arrachea, F. von Oppen, Physica E **74**, 596 (2015).
- ¹³ S. Toyabe, T. Sagawa, M. Ueda, E. Muneyuki and M. Sano, Nat. Phys. **6**, 988 (2010).
- ¹⁴ A. Berut, A. Arakelyan, A. Petrosyan, S. Ciliberto, R. Dilenschneider and E. Lutz, Nature, **483**, 187-189 (2012).
- ¹⁵ É. Roldán, I. A. Martínez, J. M. R. Parrondo and D. Petrov, Nature Phys. **10**, 457 (2014).
- ¹⁶ M. D. Vidrighin, O. Dahlsten, M. Barbieri, M. S. Kim, V. Vedral and I. A. Walmsley, Phys. Rev. Lett. **116**, 050401 (2016).
- ¹⁷ M. A. Ciampini, L. Mancino, A. Orioux, C. Vigliar, P. Matlioni, M. Paternostro and M. Barbieri, npj Quantum Inform. **3**, Article number: 10 (2017).
- ¹⁸ P. A. Camati, J. P. S. Peterson, T. B. Batalhão, K. Micadei, A. M. Souza, R. S. Sarthour, I. S. Oliveira and R. M. Serra, Phys. Rev. Lett. **117**, 240502 (2016).
- ¹⁹ J. P. S. Peterson, R. S. Sarthour, A. M. Souza, I. S. Oliveira, J. Goold, K. Modi, D. O. Soares-Pinto and L. C. Céleri, Proc. R. Soc. A **472**, 2015.0813 (2016).
- ²⁰ J. V. Koski, V. F. Maisi, T. Sagawa and J. P. Pekola, Phys. Rev. Lett. **113**, 030601 (2014).
- ²¹ J. V. Koski, V. F. Maisi, J. P. Pekola and D. V. Averin, Proc. Natl. Acad. Sci. U.S.A. **111**, 13786 (2014).
- ²² J. V. Koski, A. Kutvonen, I. M. Khaymovich, T. Ala-Nissila and J. P. Pekola, Phys. Rev. Lett. **115**, 260602 (2015).
- ²³ K. Chida, S. Desai, K. Nishiguchi and A. Fujiwara, Nat. Commun. **8**, 15301 (2017).
- ²⁴ N. Cottet, S. Jezouin, L. Bretheau, P. Campagne-Ibarcq, Q. Ficheux, J. Anders, A. Auffèves, R. Azouit, P. Rouchon and B. Huard, Proc. Natl. Acad. Sci. U.S.A. **114**, 7561 (2017).
- ²⁵ S. Hilt, S. Shabbir, J. Anders and E. Lutz, Phys. Rev. E **83**, 030102(R) (2011).
- ²⁶ A. C. Barato and U. Seifert, Europhys. Lett. **101**, 60001 (2013).
- ²⁷ P. Strasberg, G. Schaller, T. Brandes and M. Esposito, Phys. Rev. Lett. **110**, 040601 (2013).
- ²⁸ J. M. Horowitz, T. Sagawa and J. M. R. Parrondo, Phys. Rev. Lett. **111**, 010602 (2013).
- ²⁹ D. Mandal, H. T. Quan and C. Jarzynski, Phys. Rev. Lett. **111**, 030602 (2013).
- ³⁰ S. Deffner, Phys. Rev. E **88**, 062128 (2013).
- ³¹ J. J. Park, K. H. Kim, T. Sagawa and S. W. Kim, Phys. Rev. Lett. **111**, 230402 (2013).
- ³² J. Roßnagel, O. Abah, F. Schmidt-Kaler, K. Singer, and E. Lutz, Phys. Rev. Lett. **112**, 030602 (2014).
- ³³ P. Strasberg, G. Schaller, T. Brandes and C. Jarzynski, Phys. Rev. E **90**, 062107 (2014).
- ³⁴ J. Gemmer and J. Anders, New J. Phys. **17** 085006 (2015).
- ³⁵ J. P. Pekola, D. S. Golubev and D. V. Averin, Phys. Rev. B **93**, 024501 (2016).
- ³⁶ A. Kutvonen, J. Koski and T. Ala-Nissila, Scientific Reports, vol 6 , 21126 , pp. 1-7 (2016).
- ³⁷ A. V. Lebedev, D. Oehri, G. B. Lesovik, G. Blatter, Phys. Rev. A **94**, 052133 (2016).
- ³⁸ M. Campisi, J. Pekola, R. Fazio, New J. Phys. **19**, 05302 (2017).
- ³⁹ C. Elouard, D. Herrera-Martí, B. Huard, A. Auffèves, Phys. Rev. Lett. **118**, 260603 (2017).
- ⁴⁰ G. Rosselló, R. López, G. Platero, Phys. Rev. B **96**, 075305 (2017).
- ⁴¹ M. König, H. Buhmann, L. W. Molenkamp, T. L. Hughes, C.-X. Liu, X.-L. Qi, and S.-C. Zhang, J. Phys. Soc. Jpn **77**, 031007 (2008).
- ⁴² C. L. Kane and E. J. Mele, Phys. Rev. Lett. **95**, 146802 (2005).
- ⁴³ C. L. Kane and E. J. Mele, Phys. Rev. Lett. **95**, 226801 (2005).
- ⁴⁴ B. A. Bernevig, T. L. Hughes, S.-C. Zhang, Science **314**, 1757-1761 (2006).
- ⁴⁵ M. König, S. Wiedmann, C. Brune, A. Roth, H. Buhmann, L. W. Molenkamp, X.-L. Qi, and S.-C. Zhang, Science **318**, 766 (2007).
- ⁴⁶ C. Liu, T. L. Hughes, X.-L. Qi, K. Wang and S.-C. Zhang, Phys. Rev. Lett. **100**, 236601 (2008).
- ⁴⁷ L. Du, I. Knez, G. Sullivan and R.-R. Du, Phys. Rev. Lett. **114**, 096802 (2015).
- ⁴⁸ A. M. Lunde and G. Platero, Phys. Rev. B **86**, 035112 (2012).
- ⁴⁹ V. Cheianov and L. I. Glazman, Phys. Rev. Lett. **110**, 206803 (2013).
- ⁵⁰ A. Del Maestro, T. Hyart, and B. Rosenow, Phys. Rev. B **87**, 165440 (2013).
- ⁵¹ L. Kimme, B. Rosenow, and A. Brataas, Phys. Rev. B **93**, 081301(R) (2016).
- ⁵² Ch.-H. Hsu, P. Stano, J. Klinovaja, D. Loss, Phys. Rev. B **96**, 081405 (2017).
- ⁵³ A. M. Lunde and G. Platero, Phys. Rev. B **88**, 115411 (2013).
- ⁵⁴ C. Liu and S.-C. Zhang, Models and materials for topological insulators. In: *Topological Insulators*. Elsevier, 2013, p.59-86.
- ⁵⁵ I. Adagideli, V. Lutsker, M. Scheid, Ph. Jacquod and K. Richter, Phys. Rev. Lett. **108** 236601 (2012).
- ⁵⁶ C. Slichter, *Principles of Magnetic Resonance*, Springer Series in Solid-State Sciences (Springer, Berlin, 1990).
- ⁵⁷ R. I. Dzhioev and V. L. Korenev , Phys. Rev. Lett. **99**, 037401 (2007).
- ⁵⁸ S. Datta and B. Das, Appl. Phys. Lett. **56**, 665 (1990).
- ⁵⁹ G. Schmidt, D. Ferrand, L. W. Molenkamp, A. T. Filip, and B. J. van Wees, Phys. Rev. B **62**, R4790(R), (2000).
- ⁶⁰ We note that the time it takes to complete the charge/discharge cycle is only limited by the time it takes for an edge-resolved nuclear spin polarization to relax via spin-flip between nuclear spins. Nuclear spin polarization in similar systems have been reported to hold for days⁶⁴.
- ⁶¹ M. Z. Hasan and C. L. Kane, Rev. Mod. Phys. **82**, 3045

- (2010).
- ⁶² X. L. Qi and S. C. Zhang, Rev. Mod. Phys. **83**, 1057 (2011).
- ⁶³ S.-Y. Xu, L. A. Wray, Y. Xia, R. Shankar, A. Petersen, A. Fedorov, H. Lin, A. Bansil, Y. S. Hor, D. Grauer, R. J. Cava, M. Z. Hasan, arXiv:1007.5111 (2010).
- ⁶⁴ J. Tian, S. Hong, I. Miotkowski, S. Datta, Y. P. Chen, Sci. Adv. **3**, e1602531 (2017).